technologies

MDPI

Article

Reactive Spark Plasma Sintering and Mechanical Properties of Zirconium Diboride–Titanium Diboride Ultrahigh Temperature Ceramic Solid Solutions

Karthiselva N. S. and Srinivasa Rao Bakshi *

Department of Metallurgical and Materials Engineering, Indian Institute of Technology Madras, Chennai 600036, India; karthiselvas@gmail.com

* Correspondence: sbakshi@iitm.ac.in; Tel.: +91-44-2257-4781

Academic Editor: Sandip P. Harimkar

Received: 31 July 2016; Accepted: 6 September 2016; Published: 9 September 2016

Abstract: Ultrahigh temperature ceramics (UHTCs) such as diborides of zirconium, hafnium tantalum and their composites are considered to be the candidate materials for thermal protection systems of hypersonic vehicles due to their exceptional combination of physical, chemical and mechanical properties. A composite of ZrB_2-TiB_2 is expected to have better properties. In this study, an attempt has been made to fabricate ZrB_2-TiB_2 ceramics using mechanically activated elemental powders followed by reactive spark plasma sintering (RSPS) at 1400 °C. Microstructure and phase analysis was carried out using X-ray diffractometer (XRD) and electron microscopy to understand microstructure evolution. Fracture toughness and hardness were evaluated using indentation methods. Nanoindentation was used to measure elastic modulus. Compressive strength of the composites has been reported.

Keywords: ball milling; reactive spark plasma sintering; borides; UHTCs; solid solution

1. Introduction

Zirconium diboride (ZrB_2) and Titanium diboride (TiB_2) have very high melting points above 3000 °C, high hardness (>25 GPa), elastic modulus (>500 GPa), good electrical (1.0×10^7 S/m) and thermal (60–120 $W \cdot m^{-1} \cdot K^{-1}$) conductivities [1,2] and chemical stability. These physical and chemical characteristics are mandatory requirements in applications such as thermal protection systems of re-entry vehicles, crucibles and rocket nozzle [3–5]. However, fabricating fully dense compacts using conventional sintering techniques requires long processing time (>2 h) and high temperatures (>1800 °C). Apart from sintering related challenges, mechanical and oxidation resistance also needs to be improved. In order to address these issues various sintering additives such as SiC, Si_3N_4, $TiSi_2$, $MoSi_2$, TiB_2, CNT, and Graphene have been used [6–12].

TiB_2 possesses similar crystal structure (hexagonal, space group P6/mmm) and properties as ZrB_2 [13]. It has been reported that ZrB_2-TiB_2 system exhibits a complete solid solution [10,13]. Mroz [14] showed that (Ti,Zr)B_2 solid solutions exhibited higher mechanical properties than TiB_2 or ZrB_2. Aviles et al. [13] fabricated $Ti_{1-x}Zr$-B solid solutions using mechanically induced self-sustaining reactions (MSR). They have reported that solid solutions can be used to fabricate raw materials for technological applications. Inagaki et al. [15] have synthesized $Zr_{0.5}Ti_{0.5}B_2$ solid solution using hot pressing and spark plasma sintering at 1600–2200 °C. Li et al. [16] have fabricated TiB_2/ZrB_2/SiC compacts using spark plasma sintering at 1700 °C with 40 MPa applied pressure. It was reported that solid solution formation refined the microstructure and improved mechanical properties. Chakraborty et al. [17] have fabricated TiB_2-ZrB_2 based ceramics using hot pressing at 2200 °C in Ar atmosphere. They have reported that TiB_2 completely dissolves into ZrB_2 and forms a solid solution. It was also reported that mechanical and wear properties improved with addition of TiB_2 in ZrB_2.

In recent times, reactive spark plasma sintering (RSPS) has been identified as an important sintering method to fabricate ultrahigh temperature ceramics UHTCs [18–20]. Recently, we have fabricated TiB_2, ZrB_2 and TiB_2-CNT composite using RSPS at temperatures as low as 1400 °C [3,12]. Simultaneous synthesis and densification is one of the advantages of this technique. It is a very rapid process, and, hence, fine-grained bulk ceramic compacts can be fabricated. Previous research on ZrB_2-TiB_2 system shows that, in order to fabricate dense ceramic solid solutions, high temperatures as high as 2000 °C is required.

However, we have fabricated ZrB_2-TiB_2 composites using spark plasma sintering at 1500 °C having improved properties [10]. Composites were obtained using commercially available TiB_2 and ZrB_2 powders. There is no report available on fabrication of ZrB_2-TiB_2 using elemental powders followed by RSPS. Thus, the objective of the present work is to fabricate ZrB_2-TiB_2 solid solution at temperatures as low as possible. Furthermore, the solid solution formation and its effect on mechanical properties are presented.

2. Materials and Methods

Commercially pure titanium (Ti) (−325 mesh, 99.5% metal basis, Alfa Aesar, Chennai, India), zirconium (Zr) (99% pure sponge fines, <30 μm in size obtained from Nuclear Fuel Complex, Hyderabad, India), and boron (B) (amorphous powder, LobaChemie, Mumbai, India) were ball milled in a planetary ball mill (Fritsch Pulverisette-5, Germany) for 8 h. Elemental powders were taken in stoichiometric ratio and to produce ZrB_2, TiB_2 and solid solutions. Milling was carried out using tungsten carbide vials and balls (10 mm in diameter). Toluene was used as a process controlling agent. Composition details are given in Table 1. In order to find the onset of reaction between elemental powders, Differential thermal analysis (DTA) was carried out. Milled powders were heated from room temperature to 1400 °C at a heating rate of 50 °C /min.

Table 1. Microstructural details and mechanical properties of reaction spark plasma sintered samples.

Sample Name	Vol % TiB_2	Relative Density (%)	Grain Size (μm)	Nanohardness (GPa)	Elastic Modulus (GPa)	Indentation Fracture Toughness ($MPa.m^{1/2}$)
Zr-B	0	97	1.2 ± 0.25	29 ± 2	495 ± 43	3.2 ± 0.6
75Zr-25Ti-B	25	96	0.7 ± 0.30	33 ± 4	496 ± 47	3.5 ± 0.5
50Zr-50Ti-B	50	97	1.5 ± 0.50	34 ± 5	523 ± 52	3.9 ± 0.6
25Zr-75Ti-B	75	98	1.5 ± 0.40	33 ± 6	568 ± 44	3.7 ± 0.6
Ti-B	100	98	0.5 ± 0.20	34 ± 4	658 ± 32	3.4 ± 0.5

RSPS was carried out in spark plasma sintering unit (Model SPS-625, SPS Syntex Inc., Kawasaki, Japan) using 8 h milled powders at 1400 °C with a heating rate of 50 °C /min and applied pressure of 50 MPa. It should be noted that applied pressure was programmed in such a way that maximum pressure reached at highest sintering temperature. Compacts of 20 mm diameter and 5 mm thickness were fabricated using high-density graphite die. For easy removal of samples, a graphite foil (0.15 mm thickness) was inserted on the top and bottom of the powder bed and inner surface of the die. To understand the sintering behavior, the temperature, ram displacement and chamber pressure were noted as a function of time. Monolithic compacts and composites fabricated were named as Zr-B, 25Zr-75Ti-B, 50Zr-50Ti-B, 75Zr-25Ti-B, Ti-B, as described in Table 1.

Cross section samples were prepared using electro-discharge machining (EDM). Cross-sectioned samples were grounded using SiC emery sheets followed by polishing utilizing diamond paste. Water immersion technique was used to calculate bulk density. Density of the composites was calculated based on rule of mixture. An X-ray diffractometer (Panalytical, Almelo, The Netherlands) was used for phase identification. The grain size distribution and morphology were investigated using scanning electron micrograpy (FEI Quanta 400, Hillsboro, OR, USA) and InspectF (FEI, Eden Prairie, MN, USA).

Nanohardness and elastic modulus were measured using a nanoindenter (Hysitron Triboindenter (TI 950, Hysitron, Eden Prairie, MN, USA). A load of 8000 μN was used and a triangular load pattern

was used. The Oliver and Pharr model [21] was used for analysis of indentation data. Indentation fracture toughness was evaluated using Vicker's hardness tester. A load of 5 kg and dwell time of 10 s was used and the cracks formed were measured using SEM. The Anstis method [22] was used to calculate indentation fracture toughness using Equation (1):

$$K_{IC} = 0.016 \left(\frac{E}{H}\right)^{1/2} \left(\frac{P}{C^{3/2}}\right) \quad (1)$$

Room temperature compression was carried out using a Zwick universal testing machine (Zwick, Ulm, Germany). Samples having dimensions of 6 mm height and 3.5 mm width were used for the compression testing.

3. Results and Discussion

3.1. Mechanical Milling and Thermal Analysis

Figure 1 shows 0.5 h ball milled elemental powders. It shows that no impurity material signatures were observed other than starting elemental powders. However, presence of small amount of monoclinic zirconium dioxide (ZrO_2) was observed. It should be noted that amorphous boron was used, and, hence, it was not observed in the x-ray diffractogram. From Figure 2, slight peak shifting and broadening are observed after 8 h of ball milling. This is due to the milling induced lattice strain and reduction in crystallite size. Reactions among elemental Zr-B and Ti-B is highly exothermic in nature. However, TiB_2 and ZrB_2 peaks were not observed after 8h of milling. Toluene was used as a process controlling medium and it prevented temperature rise and reaction between the powders. However, monoclinic ZrO_2 peak intensity decreased and small tungsten carbide (WC) peak observed after 8 h milling.

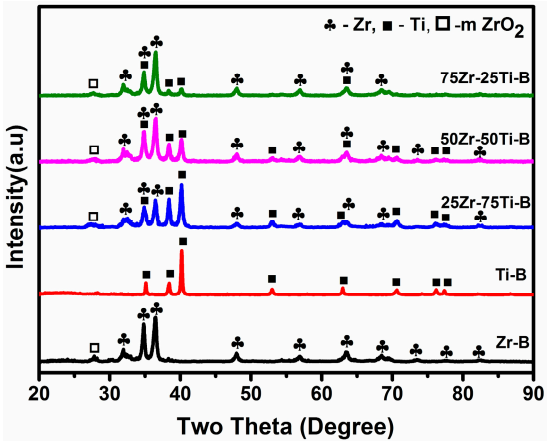

Figure 1. X-ray diffractogram of 0.5 h ball milled elemental powders.

Differential scanning calorimetry plot of 8 h mechanically milled elemental powders is shown in Figure 3. The first exothermic peak observed between 900 and 1000 °C corresponds to α phase to β phase transition of Ti and Zr. The second exothermic peak which occurs in the range of 1000–1300 °C corresponds to formation of ZrB_2 and TiB_2. Thus, 1400 °C was chosen as sintering temperature to fabricate compacts. It should be noted that the onset of exothermic reaction varies with addition of Zr or Ti.

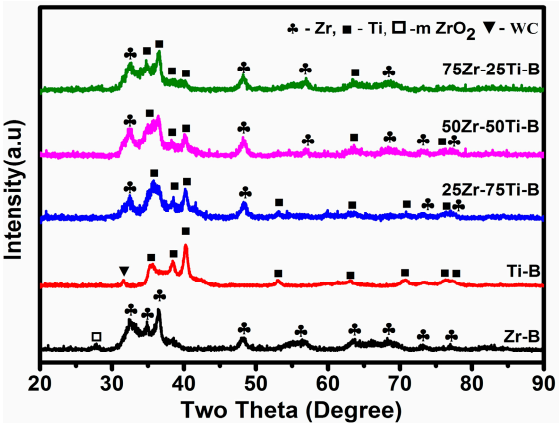

Figure 2. XRD of 8 h ball milled elemental powders.

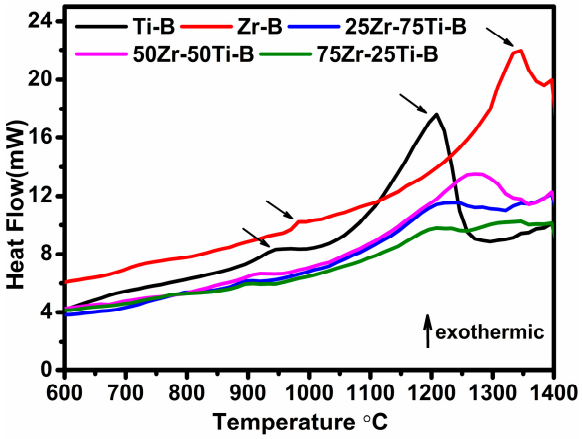

Figure 3. Differential scanning calorimetry (DSC) traces of elemental powder mixtures milled for 8 h.

3.2. Simultaneous Synthesis and Densification

During RSPS, a sudden increase in punch displacement was observed in the temperature range of 550–700 °C. During this time, an an intense flash of light appeared on the top and bottom of the die punches. This kind of phenomenon was observed during our earlier studies as well. High exothermic reaction between the elemental powders is the reason for this occurrence of the flash, and sudden displacement. To understand this phenomenon, the sample displacement, temperature, time and pressure during RSPS were analysed. Figure 4 shows the plot of displacement behaviour of 8 h milled elemental powders during RSPS. The sample displacement reported in the present study includes contribution from graphite dies, punches, and spacers. Tamburini et al. [23] reported a method to subtract this complex displacement, and it can be found elsewhere. However, in the present study, it is difficult to remove this contribution from sample displacement due to following reasons. In the present study, we have used RSPS in which self-propagating high temperature synthesis reaction (SHS) induced sample displacement occurs and this facilitates faster densification. Due to the excessive heat released during this event, graphitic die, punches and spacers may expand and during cooling it may contract. Thus, it is very difficult to subtract from the data.

It can be observed that, there are four distinct stages in the plot; (1) initial sintering stage (2) SHS reaction region (3) additional sintering stage (4) minor densification stage. In the initial stage, gradual shrinkage due to particle rearrangement was observed. During the second stage, sudden displacement change observed in all the samples. This was due to highly exothermic reaction between the milled powders.

The adiabatic temperature of TiB_2 and ZrB_2 is above 3000 K, which is above the threshold limit of 1800 K value of SHS reaction to occur [24]. During the exothermic reaction, a very high temperature is released, which is sufficient to convert milled powders to products. Similar phenomena was reported by us earlier [3,4]. The Zr-B sample showed this phenomenon at ~300 s, while the Ti-B samples showed this at 440 s. From Figure 3, it was observed that exothermic reaction was observed in the temperature range of 1000–1300 °C, but, during RSPS, SHS induced sudden displacement occurred in the temperature range of 550–700 °C. This indicates that effect of current, applied pressure played a role in enhanced kinetics during RSPS. In the third stage, additional densification was observed where plastic flow is the main densification mechanism. In our earlier study, it was showed that plastic flow controlled the densification [3]. It should be noted that additional densification was not observed in Ti-B and for Zr-B. The magnitude of additional densification is observed to decrease with the increase in vol. % of TiB_2. It indicates that addition of TiB_2 modifies the sintering mechanism. In the fourth stage, minor densification occurs.

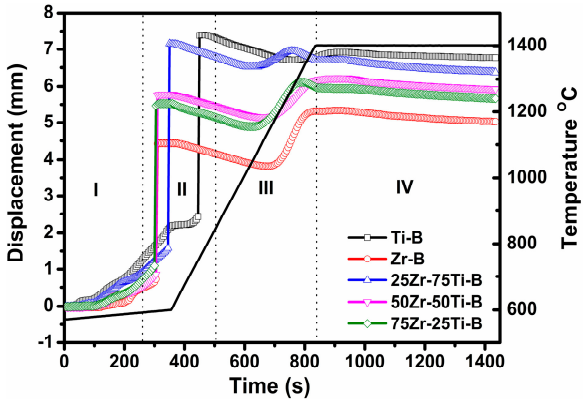

Figure 4. Sintering behavior at 1400 °C with 50 MPa applied pressure and 50 °C/min heating rate.

3.3. Phase Analysis and Microstructural Characterisation

The XRD patterns of RSPSed samples are shown in Figure 5. Formation of TiB_2 and ZrB_2 and intermediate phase TiB was observed. The 75Zr-25Ti-B, 50Zr-50Ti-B and 25Zr-75Ti-B exhibited solid solution formation. It is well-known that ZrB_2-TiB_2 system forms a perfect solid solution [25]. The atomic radius difference between Ti and Zr is only 9%. Solid solution formation was reported by various research groups [13,17]. Peak shifting and broadening of peaks was observed in 75Zr-25Ti-B, 50Zr-50Ti-B and 25Zr-75Ti-B as compared to monolithic TiB_2 and ZrB_2. It should be noted that TiB_2 (a = 3.029 Å, c = 3.228 Å) unit cell is smaller than ZrB_2 (a = 3.170 Å, c = 3.530 Å) [17].

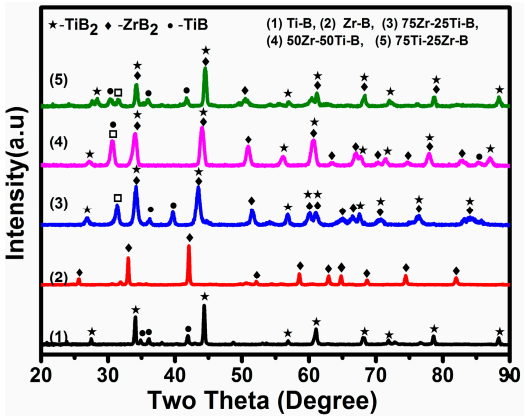

Figure 5. XRD of RSPSed samples.

Addition of TiB_2 in ZrB_2 shifted the peaks to higher angles, and this is due to decrease in lattice parameter due to dissolution of Ti in Zr. The 50Zr-50Ti-B sample exhibited a complete solid solution while the 75Zr-25Ti-B and 25Zr-75Ti-B samples showed residual ZrB_2 or TiB_2. The presence of TiB and ZrO_2 was also observed [3,4].

The SEM backscattered electron micrographs of Zr-B, Ti-B and 50Zr-50Ti-B shown in Figure 6 indicate that dense, pore-free microstructure can be obtained. Brighter regions in 50Zr-50Ti-B represent ZrB_2 rich phase, and a darker phase corresponds to the TiB_2 rich phase.

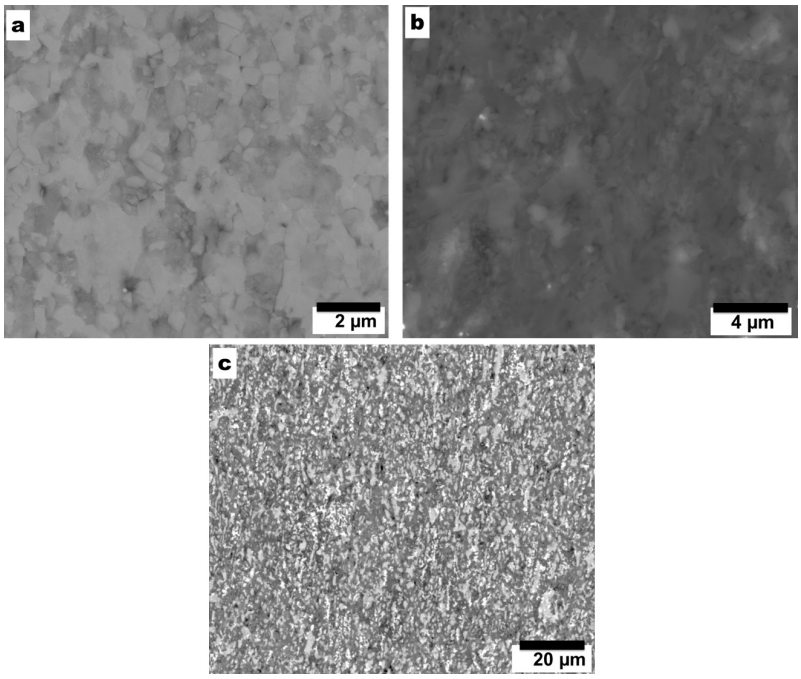

Figure 6. SEM back scattered electron (BSE) images showing the microstructure (**a**) Zr-B; (**b**) Ti-B; and (**c**) 50Zr-50Ti-B.

Fracture surfaces of RSPSed samples are shown in Figure 7. It can be clearly observed that grain size is less than micron size in Ti-B compared to all other compositions. The intermediate product TiB acted as a grain pinning agent and arrested grain growth. In all other cases, it is evident that densification and grain growth occurred simultaneously. However, the average grain size of all the samples is less than 2 µm. It is reported that TiB_2 dissolves into ZrB_2 along the phase boundary and restricts grain growth [26]. The measured grain sizes are tabulated in Table 1. It should be noted that fabrication of dense, fine-grained solid solution compacts of UHTCs is a challenging task. The bulk density of all the samples were measured and presented in Table 1. In the present study, we show that more than 95% dense compacts of UHTC solid solution can be prepared at low temperature of 1400 °C using the RSPS method.

3.4. Mechanical Characterisation

Indentation fracture toughness was measured for all the RSPSed compacts and the values are plotted in Figure 8. It is observed that high indentation fracture toughness values are exhibited by solid solution compositions compared to monolithic samples. This clearly indicates that a solid solution formation has a prominent effect on mechanical properties. Figure 9 shows the representative Vicker's indentation and the generated cracks showing crack tortuosity.

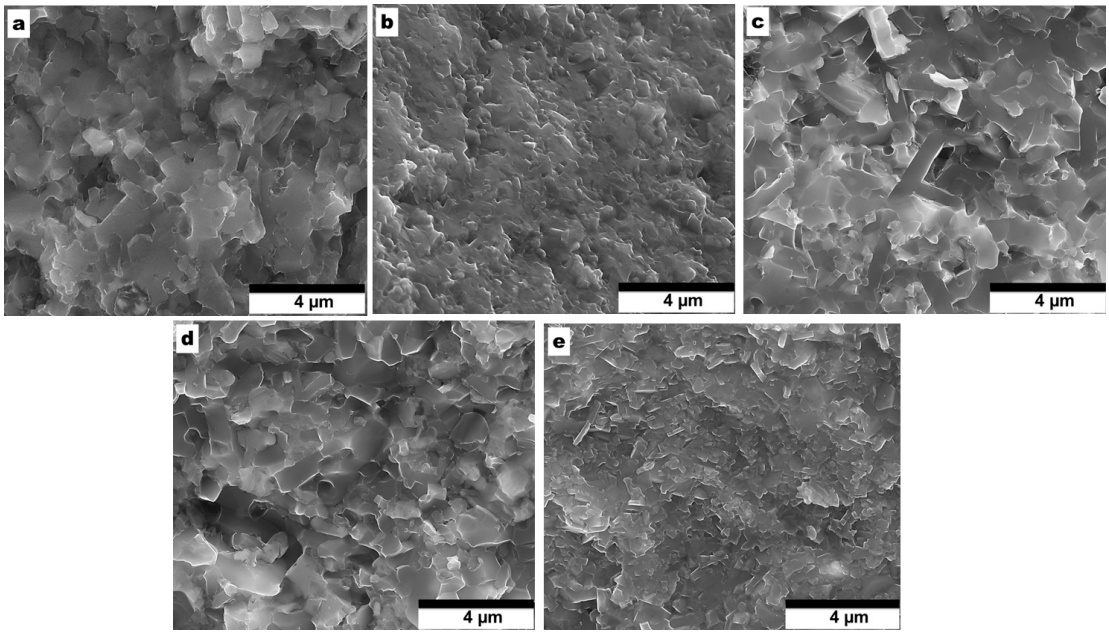

Figure 7. Fracture surfaces of RSPSed samples (**a**) Zr-B; (**b**) 75Zr-25Ti-B; (**c**) 50Zr-50Ti-B; (**d**) 25Zr-75Ti-B; and (**e**) Ti-B.

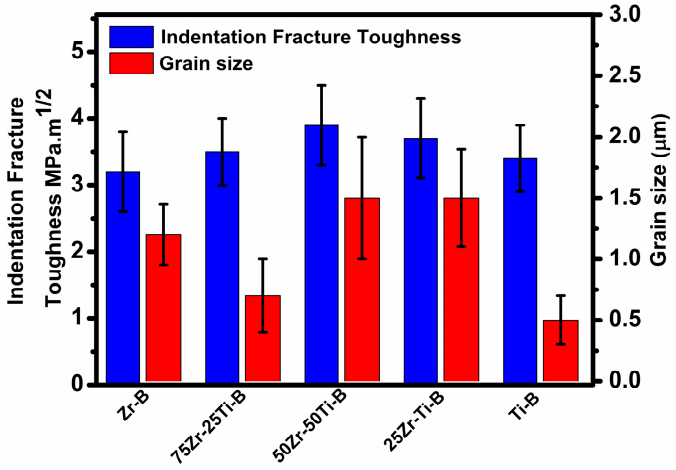

Figure 8. Grain size and indentation fracture toughness of RSPSed samples.

Figure 9b,d show crack branching and deflection phenomena. The 50Zr-50Ti-B showed high fracture toughness compared to other compositions. Considering the different coefficient of thermal expansion (CTE) of ZrB_2 (α_a = 6.66, $\alpha_c = 6.93 \times 10^{-6}$ K^{-1}) and TiB_2 (α_a = 6.36, $\alpha_c = 9.30 \times 10^{-6}$ K^{-1}), residual stress toughening can also be an important toughening mechanism. Residual stresses can generate microcracks during cooling stage of RSPS. These microcracks dissipate strain energy of main crack and enhance fracture toughness [26]. Based on the energy principle, when solid solution forms Ti^+, is replaced with Zr^+, and the internal energy may increase. Moreover, solid solution reaction occurs at the interphase; hence, due to reduced movement of grain boundary, grain size reduction occurs and improves the mechanical properties [16].

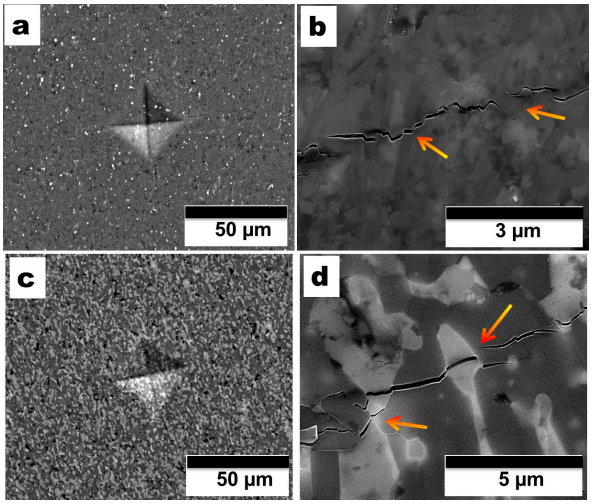

Figure 9. Representative Vickers indentation pattern showing cracks and toughening mechanisms. (**a**,**c**) Vicker's indentation pattern of (**a**) Ti-B; (**c**) 75Zr-25Ti-B. Crack branching, deflection showed in (**b**) Ti-B; (**d**) 75Zr-25Ti.

Figure 10 shows the room temperature compressive strength of RSPSed compacts. The 50Zr-50Ti-B sample showed high compressive strength, which clearly indicates that the solid solution formation has a pronounced effect on mechanical properties. Figure 11 shows the high temperature compressive strength data of Zr-B and 50Zr-50Ti-B samples. There was no significant change observed in both compositions and machine reached its safety limit. It can be said that the solid solution may exhibit better high temperature strength.

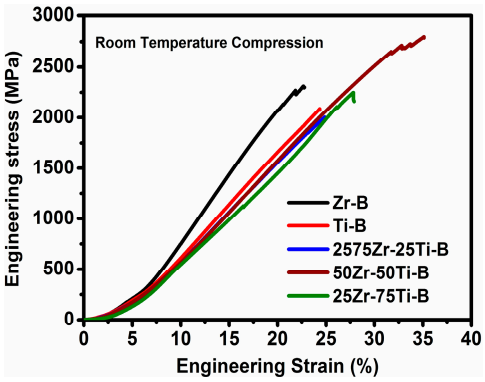

Figure 10. Room temperature compressive strength of RSPSed samples.

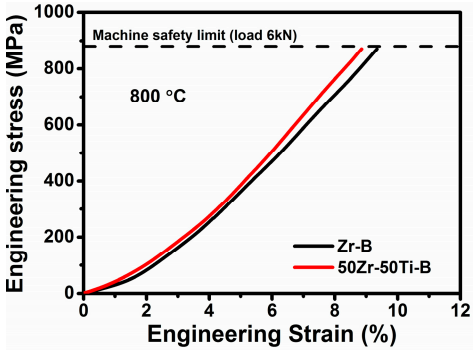

Figure 11. High temperature compressive strength of RSPSed samples.

Figure 12 shows the representative loading vs. displacement profile of nanoindentation. Measured nanohardness and elastic modulus is reported in Table 1. It can be observed from Table 1 that the hardness and elastic modulus increases with increase in TiB_2 content. Figure 12 shows the pop-in phenomenon in 50Zr-50Ti-B sample. This phenomenon could happen due to various reasons: (1) phase transformation; (2) dislocation generation under the indenter; and (3) critical resolved shear stress being reached at that particular load. A similar kind of pop-in phenomenon was observed by Guicciardi et al. [27] in the ZrB_2-SiC composite. They have reported that pop-in was observed when the indentations were made inside the grains. This indicates at room temperature small scale plasticity has been exhibited by 50Zr-50Ti-B. However, more investigations need to be carried out in order to investigate slip- or twin-system activation under the indenter. The mechanical properties of the compacts are found to be similar to those reported in the literature. However, thorough mechanical property characterization and oxidation property evaluation has to be carried out as future work to use these compositions for UHTC applications.

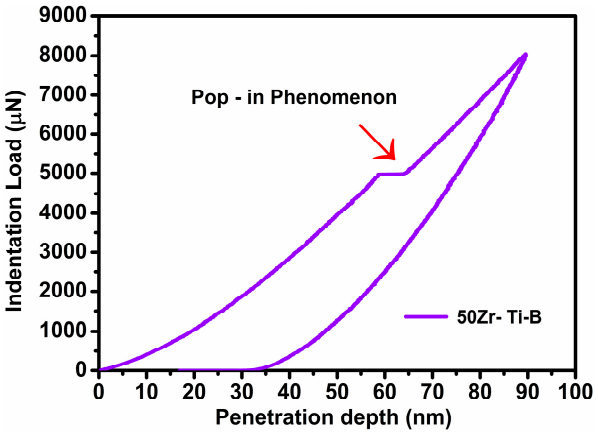

Figure 12. Load vs. displacement profile of 50Zr-50Ti-B sample.

RSPS reduces sintering time and temperature and hence is an energy efficient method. Licheri et al. [28] have discussed few safety aspects related to RSPS process. Firstly, the die, punches and spacers can get damaged due to the very high and rapid energy release in the contained environment. Secondly, there can be expulsion of powders during SHS reaction. Thirdly, entrapped gases may cause porosity, which may be difficult to remove during later stages of sintering. It was recommended that the sudden displacement should be avoided to prevent die damage. However, we have observed that there is no die damage when we increase pressure linearly with temperature instead of applying the load in the beginning. In addition, a lower heating rate of up to 100 °C/min is found to be safe. We have also shown that the addition of the second phase, such as carbon nanotubes, also inhibits the SHS reaction [12]. Thus, it is seen that RSPS can be an attractive low temperature method for fabricating dense, fine-grained compacts of ultrahigh temperature ceramics and their solid solutions.

4. Conclusions

(1) Monolithic ZrB_2, TiB_2 and solid solution compacts were successfully fabricated using RSPS of 8 h ball milled elemental powder mixtures at temperatures as low as 1400 °C with 50 MPa applied pressure. The fracture surface images showed fine-grained microstructure (<2 μm).

(2) Two major different densification mechanisms were active during RSPS: (1) SHS reaction (2) plastic flow aided densification.

(3) XRD results revealed solid solution formation. The 50Zr-50Ti-B exhibited a perfect solid solution while other compositions showed residual phases.

(4) Solid solution samples showed high indentation fracture toughness due to various toughening mechanisms such as crack deflection and crack branching.

(5) The nanohardness, elastic modulus and compressive strength were improved with solid solution formation. Pop-in phenomenon exhibited by 50Zr-50Ti-B during nanoindentation.

Acknowledgments: Srinivasa Rao Bakshi would like to acknowledge funding from IIT Madras New Faculty Seed Grant (MET/11-12/547/NFSC/SRRB) for carrying out this research. Authors acknowledge help of N. Saibaba, Director of Nuclear Fuel Complex in Hyderabad, India for providing zirconium powder. Authors would like to thank B. S. Murty for providing facilities to carry out the research.

Author Contributions: K.N.S. and S.R.B. conceived and designed the experiments; K.N.S. performed the experiments; K.N.S. and S.R.B. analyzed the data; K.N.S. wrote the paper and S.R.B. contributed to writing. All the authors read and accepted the final manuscript.

Conflicts of Interest: The authors declare that there is no conflict of interest.

References

1. Basu, B.; Raju, G.B.; Suri, A.K. Processing and properties of monolithic TiB_2 based materials. *Int. Mater. Rev.* **2006**, *51*, 352–374. [CrossRef]
2. Fahrenholtz, W.G.; Wuchina, E.J.; Lee, W.E.; Zhou, Y. (Eds.) *Ultra-High Temperature Ceramics: Materials for Extreme Environment Applications*; John Wiley & Sons, Inc.: Hoboken, NJ, USA, 2014.
3. Karthiselva, N.S.; Murty, B.S.; Bakshi, S.R. Low temperature synthesis of dense and ultrafine grained zirconium diboride compacts by reactive spark plasma sintering. *Scr. Mater.* **2016**, *110*, 78–81. [CrossRef]
4. Karthiselva, N.S.; Murty, B.S.; Bakshi, S.R. Low temperature synthesis of dense TiB_2 compacts by reaction spark plasma sintering. *Int. J. Ref. Met. Hard Mater.* **2015**, *48*, 201–210. [CrossRef]
5. Yadhukulakrishnan, G.B.; Rahman, A.; Karumuri, S.; Stackpoole, M.M.; Kalkan, A.K.; Singh, R.P.; Harimkar, S.P. Spark plasma sintering of silicon carbide and multi-walled carbon nanotube reinforced zirconium diboride ceramic composite. *Mater. Sci. Eng. A* **2012**, *552*, 125–133. [CrossRef]
6. Patel, M.; Singh, V.; Reddy, J.J.; Bhanu Prasad, V.V.; Jayaram, V. Densification mechanisms during hot pressing of ZrB_2–20 vol.% SiC composite. *Scr. Mater.* **2013**, *69*, 370–373. [CrossRef]
7. Monteverde, F.; Guicciardi, S.; Bellosi, A. Advances in microstructure and mechanical properties of zirconium diboride based ceramics. *Mater. Sci. Eng. A* **2003**, *346*, 310–319. [CrossRef]
8. Golla, B.R.; Basu, B. Hot-pressed TiB_2–10 wt.% $TiSi_2$ ceramic with extremely good thermal transport properties at elevated temperatures (up to 1273K). *Scr. Mater.* **2013**, *68*, 79–82. [CrossRef]
9. Raju, G.B.; Mukhopadhyay, A.; Biswas, K.; Basu, B. Densification and high-temperature mechanical properties of hot pressed TiB_2–(0–10 wt.%) $MoSi_2$ composites. *Scr. Mater.* **2009**, *61*, 674–677. [CrossRef]
10. Karthiselva, N.S.; Murty, B.S.; Bakshi, S.R. Densification and mechanical properties of ZrB_2-TiB_2 ultra high temperature ceramic composites. In *Developments in Strategic Materials and Computational Design V: A Collection of Papers*, Proceedings of the 38th International Conference on Advanced Ceramics and Composites, Daytona Beach, FL, USA, 27–31 January 2014; Volume 35, pp. 275–285.
11. Yadhukulakrishnan, G.B.; Karumuri, S.; Rahman, A.; Singh, R.P.; Kaan Kalkan, A.; Harimkar, S.P. Spark plasma sintering of graphene reinforced zirconium diboride ultra-high temperature ceramic composites. *Ceram. Int.* **2013**, *39*, 6637–6646. [CrossRef]
12. Karthiselva, N.S.; Bakshi, S.R. Carbon nanotube and in-situ titanium carbide reinforced titanium diboride matrix composites synthesized by reactive spark plasma sintering. *Mater. Sci. Eng. A* **2016**, *663*, 38–48. [CrossRef]
13. Avilés, M.A.; Córdoba, J.M.; Sayagués, M.J.; Gotor, F.J. Mechanochemical synthesis of $Ti_{1-x}Zr_xB_2$ and $Ti_{1-x}Hf_xB_2$ solid solutions. *Ceram. Int.* **2011**, *37*, 1895–1904. [CrossRef]
14. Mroz, C. Processing and Properties of Microcomposite TiZrC and $TiZrB_2$ Materials. In *17th Annual Conference on Composites and Advanced Ceramic Materials, Part 2 of 2: Ceramic Engineering and Science Proceedings*; John Wiley & Sons, Inc.: Hoboken, NJ, USA, 1993; Volume 14, pp. 725–735.
15. Inagaki, J.-I.; Sakai, Y.; Uekawa, N.; Kojima, T.; Kakegawa, K. Synthesis and evaluation of $Zr_{0.5}Ti_{0.5}B_2$ solid solution. *Mater. Res. Bull.* **2007**, *42*, 1019–1027.
16. Li, B. Effect of ZrB_2 and SiC addition on TiB_2-based ceramic composites prepared by spark plasma sintering. *Int. J. Ref. Met. Hard Mater.* **2014**, *46*, 84–89. [CrossRef]

17. Chakraborty, S.; Debnath, D.; Mallick, A.R.; Das, P.K. Mechanical and thermal properties of hot pressed ZrB_2 system with TiB_2. *Int. J. Ref. Met. Hard Mater.* **2014**, *46*, 35–42. [CrossRef]
18. Licheri, R.; Orrù, R.; Musa, C.; Cao, G. Combination of SHS and SPS Techniques for fabrication of fully dense ZrB_2-ZrC-SiC composites. *Mater. Lett.* **2008**, *62*, 432–435. [CrossRef]
19. Musa, C.; Orrù, R.; Licheri, R.; Cao, G. Spark plasma synthesis and densification of TaB_2 by pulsed electric current sintering. *Mater. Lett.* **2011**, *65*, 3080–3082. [CrossRef]
20. Rehman, S.S.; Ji, W.; Fu, Z.; Wang, W.; Wang, H.; Asif, M.; Zhang, J. In situ synthesis and sintering of B_4C/ZrB_2 composites from B_4C and ZrH_2 mixtures by spark plasma sintering. *J. Eur. Ceram. Soc.* **2015**, *35*, 1139–1145. [CrossRef]
21. Oliver, W.C.; Pharr, G.M. An improved technique for determining hardness and elastic modulus using load and displacement sensing indentation experiments. *J. Mater. Res.* **1992**, *7*, 1564–1583. [CrossRef]
22. Anstis, G.R.; Chantikul, P.; Lawn, B.R.; Marshall, D.B. A Critical Evaluation of Indentation Techniques for Measuring Fracture Toughness: I, Direct Crack Measurements. *J. Am. Ceram. Soc.* **1981**, *64*, 533–538. [CrossRef]
23. Anselmi-Tamburini, U.; Garay, J.E.; Munir, Z.A. Fundamental investigations on the spark plasma sintering/synthesis process. *Mater. Sci. Eng. A* **2005**, *407*, 24–30. [CrossRef]
24. Su, X.; Fu, F.; Yan, Y.; Zheng, G.; Liang, T.; Zhang, Q.; Cheng, X.; Yang, D.; Chi, H.; Tang, X.; et al. Self-propagating high-temperature synthesis for compound thermoelectrics and new criterion for combustion processing. *Nat. Commun.* **2014**, *5*, 4908. [CrossRef] [PubMed]
25. Yin, J.; Huang, Z.; Liu, X.; Yan, Y.; Zhang, H.; Jiang, D. Mechanical properties and in-situ toughening mechanism of pressurelessly densified ZrB_2–TiB_2 ceramic composites. *Mater. Sci. Eng. A* **2013**, *565*, 414–419. [CrossRef]
26. Yin, J.; Zhang, H.; Yan, Y.; Huang, Z.; Liu, X.; Jiang, D. High toughness in pressureless densified ZrB_2-based composites co-doped with boron–titanium carbides. *Scr. Mater.* **2012**, *66*, 523–526. [CrossRef]
27. Guicciardi, S.; Melandri, C.; Monteverde, F.T. Characterization of pop-in phenomena and indentation modulus in a polycrystalline ZrB_2 ceramic. *J. Eur. Ceram. Soc.* **2010**, *30*, 1027–1034. [CrossRef]
28. Licheri, R.; Musa, C.; Orrù, R.; Cao, G. Influence of the heating rate on the in situ synthesis and consolidation of ZrB_2 by reactive Spark Plasma Sintering. *J. Eur. Ceram. Soc.* **2015**, *35*, 1129–1137. [CrossRef]